Contractile response of alveolar epithelial cells to biochemical or mechanical stimulation probed by traction microscopy

Núria Gavara i Casas

Contractile response of alveolar epithelial cells to biochemical or mechanical stimulation probed by traction microscopy

A dissertation by
Núria Gavara i Casas
in partial fulfilment of the requirements for
the degree of Doctor of Philosophy

Thesis supervisor : Prof. Ramon Farré i Ventura

Unitat de Biofísica i Bioenginyeria
Dept. de Ciències Fisiològiques I
Facultat de Medicina, Universitat de Barcelona.

Chapter 5. Stretch-induced contraction of alveolar epithelial cells

5.1 Introduction

Adherent living cells experience a variety of mechanical stresses that regulate fundamental cellular functions such as growth, spreading, migration, mechanotransduction, differentiation, apoptosis and protein synthesis (Chicurel et al., 1998;Janmey, 1998;Huang and Ingber, 1999). In particular, alveolar epithelial cells are believed to undergo stretches of 5-10% under physiological breathing conditions. This stretch may be dramatically increased in patients with acute respiratory failure receiving mechanical ventilation, reaching 15-25% strain levels (Liu et al., 1999;Tschumperlin and Margulies, 1999;Wirtz and Dobbs, 2000;Vlahakis and Hubmayr, 2003). Mechanical ventilation with high volumes and pressures can either cause de novo lung injury or aggravate preexisting lung injury (Dreyfuss and Saumon, 1998;Ricard et al., 2003). This pathological result, known as ventilator-induced lung injury (VILI), is characterized by formation or worsening of alveolar air leaks, presence of protein-rich alveolar edema and alveolar cell dysfunction. Therefore, excessive deforming stresses associated with mechanical ventilation could impair alveolar epithelial barrier function and produce increased paracellular permeability (Cavanaugh et al., 2006).

The physical integrity of the alveolar epithelial cell monolayer is governed by a dynamic force balance at the cell-cell and cell-matrix attachments between centripetal cell mechanical tension and centrifugal adhesive forces (Dudek and Garcia, 2001). Mechanical tension arises from both active contraction generated by the actomyosin machinery and

passive elastic recoil caused by cyclic stretching due to breathing or mechanical ventilation. Maintenance of the cell monolayer under stretch conditions requires tethering adhesive forces to withstand active and passive tension.

It has been shown that cyclic stretch in the range corresponding to high lung volume ventilation induces significant increase in paracellular permeability (Cavanaugh et al., 2006). Consequently, stretch must modify some of the force components involved in alveolar cell monolayer integrity. Previous work from our laboratory has shown that stretch induced a significant increase on cell stiffness in a dose dependent manner (Trepat et al., 2004). Besides, it has been reported that 17% cyclic stretch induced changes in tethering adhesive forces, with significant decreases in the intensity of peripheral occludin, the degree of cell–cell attachment, and total cellular occluding content (Cavanaugh, Jr. et al., 2001). Nevertheless, no direct data are available to conclusively determine the effect of stretch in the contractile properties of alveolar epithelial cells. On the one hand, intracellular Ca^{2+} levels have been shown to display a fast and transient increase after a single stretch application, suggesting activation of the acto-myosin machinery (Wirtz and Dobbs, 1990). On the other hand, it has been suggested that a step-wise stretch could induce disruption of actin-myosin interactions and cytoskeletal crosslinks (Trepat et al., 2006), potentially reducing active force generation. Therefore, direct measurements of stretch-induced changes in traction forces exerted by alveolar epithelial cells are required for better understanding the role of active contraction on the force balance that regulates alveolar barrier permeability under mechanical ventilation conditions.

Few data are available on the effect of stretch on the contractility of adherent cells, mainly due to technical reasons. Munevar and coworkers (Munevar et al., 2004) reported that stretch induced increases in traction forces and intracellular Ca^{2+} concentration in fibroblasts. Nevertheless, stretch was applied by locally deforming the flexible substrate in the vicinity of the cell with a blunted tip and traction forces were measured after tip removal. Therefore, the experimental setup used by these authors did not allow for application of controlled biaxial strain levels similar to that in the alveoli or measurement of traction forces during stretch. Consequently, a novel experimental approach which enables application of controlled biaxial stretch and simultaneous measurement of traction forces is required to better characterize the effect of stretch on cell contractility.

The aim of this work was to study the contractile response induced by physiological stretch levels on alveolar epithelial cells. To this end, we developed and characterized a novel device capable of subjecting cells to uniform, equibiaxial strains and simultaneously measure exerted traction forces. The device was based on combining two established techniques, namely equibiaxial substrate stretching (Trepat et al., 2004) and traction microscopy (Butler et al., 2002). Cell stretching was produced by distending a collagen gel attached to a flexible substrate with a vacuum-driven device mounted on an epi-fluorescence microscope. Applied strain and traction forces exerted by the cell were measured from local gel deformations by tracking the displacement of small fluorescent beads embedded in the collagen gel. The contractile response of alveolar epithelial cells was studied for two different stretch levels, both during stretch application and after stretch release. We also studied possible mechanisms responsible for the observed contractile response. Stretch-induced changes in actin polymerization where assessed by quantifying F/G-actin ratio. Stretch-induced disruption of actin-myosin interactions was studied by pre-treating the cells with ML-7, a myosin light chain kinase (MLCK) inhibitor. Finally, active recovery of cell contractility was assessed by recording time-course of traction forces after stretch release.

5.2 Materials and methods

5.2.1 Materials

Tissue culture medium RPMI 1640, L-glutamine, penicillin and streptomycin were obtained from GIBCO (Gaithersburg, MD), fetal calf serum from Biological Industries (Kibbutz Beit Haemek, Israel) and collagen I from Upstate (Lake Placid, NY). Unless otherwise specified, reagents were purchased from Sigma Chemical Co. (St. Louis, MO). Fluorescent latex beads and Alexa Fluor 488 DNase I conjugate were supplied by Molecular Probes (Eugene, OR).

5.2.2 Cell culture

The study was carried out on human alveolar epithelial cells A549, culture line CCL-185 (ATCC, Manassas, VA). Cells were cultured in HEPES buffered RPMI 1640 with 10% inactivated fetal calf serum, 1mM L-glutamine, 100 U/ml penicillin, 100 mg/ml streptomycin (GIBCO, Gaithersburg, MD) and 2 μg/ml amphotericin B. One day before traction microscopy experiments, cells were detached by means of a brief exposure to trypsin EDTA and plated sparsely on collagen gels (3×10^4 cells/gel) attached to flexible-bottomed culture wells (35 mm diameter; Bioflex, Flexcell International, PA). The culture medium was replaced by serum-free medium before the experiment. For actin staining experiments, cells were plated (3×10^5 cells/well) on collagen I-coated flexible-bottomed culture wells. Actin staining measurements were performed at confluence 4 days after plating.

5.2.3 Stretching device

Device description

Collagen gels with embedded fluorescent microbeads were used as transparent, elastic and stretchable cell substrates. Collagen gels were firmly attached to flexible-bottomed culture wells. To stretch the gels, we adapted a previously described stretching device, based on applying vacuum underneath a flexible-bottomed well (Trepat et al., 2004) (Fig. 5.1). Deformations of the bottom of the well were transmitted to the collagen gel. The system was mounted on an inverted fluorescence microscope (Eclipse TE2000, Nikon, Japan) placed on a vibration isolation table (Isostation, Newport, Irvine, CA). To obtain equibiaxial and uniform strains in the central region of the substrate, a cylindrical loading post was located beneath the well (Schaffer et al., 1994;Hung and Williams, 1994). When a negative pressure was applied under the annular outer region of the substrate, the central area was stretched. The rising and falling times of the applied pressure step were modulated by a resistor-capacitor pneumatic filter inserted between the sample and a vacuum source, resulting in a time constant of ~2 seg. The stretching device was designed to allow for combination with a home-made AFM, thus enabling simultaneous stretch application and stiffness measurements (Fig. 5.1).

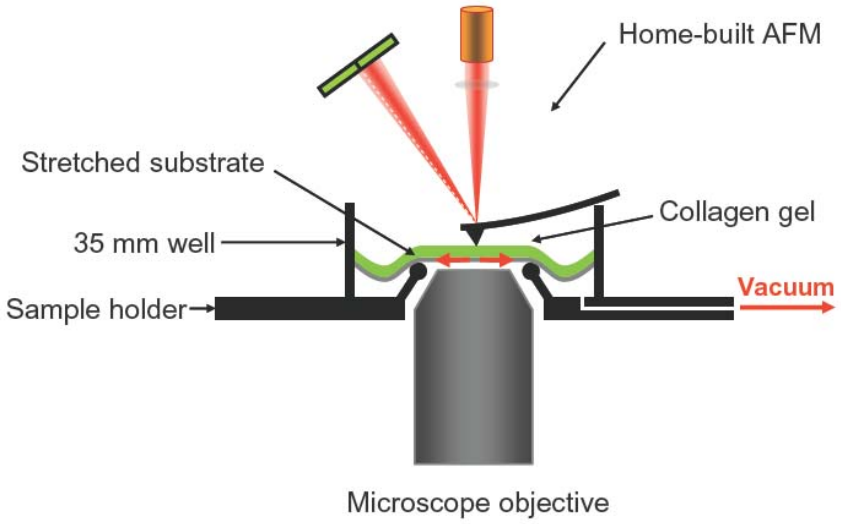

Fig. 5.1 Sketch of the experimental setup. Collagen gels with embedded fluorescent microbeads were allowed to polymerize on flexible-bottomed wells. The wells were positioned on a sample holder based on a hollow cylindrical loading-post concentric with the objective of the epi-fluorescence microscope. The application of a negative pressure underneath the annular outer region of the sample resulted in a homogeneous and equibiaxial strain of the central area. The stretching device allowed measurement of the gel's stiffness using a home-made atomic force microscope.

Device calibration

To measure the relationship between applied vacuum underneath the well and resulting gel deformation, fluorescence images of the microbeads at the top of the gel were used. A central region of the gel was selected and fluorescence images were acquired using a 12-bit resolution cooled-CCD camera (Orca AG, Hamamatsu Photonics, Japan) at 20× magnification. The substrate was progressively deformed with negative pressure steps of 50 mmHg up to 350 mmHg. After each increase in substrate deformation, the selected region of the gel was relocated into the field of view and the gel surface was refocused before fluorescence images acquisition. Finally, the vacuum was released and a second image of the relaxed gel was acquired. Measurements were carried out in 5 different gel samples. Strain was computed from the displacement of the fluorescent microbeads between the stretched and the relaxed images as described on the data processing section below.

5.2.4 Traction microscopy

Collagen gels

Collagen gelation was performed on the surface of collagen-coated flexible-bottomed culture wells following a previously described method (Haga et al., 2005). The protocol to produce 1.45 mg/ml collagen gels is extensively described in Appendix B.

Measurement of the Young's modulus of the gels

Young's modulus (E) of collagen gels subjected to different strain levels was measured with Atomic Force Microscopy (AFM) using a previously described method (Alcaraz et al., 2003). The spring constant of the AFM cantilever was calibrated by the thermal fluctuations method in water (Burnham et al., 2003). For each selected region of a gel sample, strain was progressively increased with steps of 5.5% strain up to 11% strain, and a set of 10 force-displacement curves were recorded at a single point for each applied strain. Subsequently, the stretch was released and the cantilever was moved to a different gel region, where the stretching procedure was repeated. Measurements were carried out on 5 distant gel regions of 5 gel samples. Young's modulus was computed from the force-displacement curves (Bilodeau, 1992) using non-linear least squares regression. For each gel sample and strain level, the value of E was taken as the average of the five measurements done at different gel regions.

5.2.5 Microscopy

The flexible-bottomed wells containing cell-cultured collagen gels were fitted in the stretching device, which was mounted on the stage of an inverted fluorescence microscope (Eclipse TE2000, Nikon, Japan) placed on a vibration isolation table (Isostation, Newport, Irvine, CA). Bright field and fluorescence images were acquired with a 12-bit resolution cooled-CCD camera (Orca AG, Hamamatsu Photonics, Japan). The apparent pixel size after magnification (20×) was 0.32 μm with a resulting field of view of 323×323 μm^2.

5.2.6 Measurements

Traction microscopy protocol

The traction microscopy protocol is illustrated in Fig. 5.2. A well containing cell-cultured collagen gel was placed on the stretching device and imaged with bright field illumination. A bright field image of an isolated cell was captured to determine its boundary. Subsequently, the apical surface of the gel was focused and a fluorescence image of the microbeads embedded near the surface of the gel was acquired (Fig. 5.2 I). The well was stretched and bright field and fluorescence image acquisition of the studied cell was performed again (II). Subsequently, the stretch was released and two final bright field and fluorescence images of the cell were acquired (III). Once the cell was removed from the gel by exposure to trypsin, a fluorescence image was recorded to determine the position of the beads in the cell-free unstrained gel (IV). The gel was then stretched again, and a fluorescence image was recorded to observe the beads' position in the cell-free strained gel (V). Stretching-unstretching of the cell-free gel was repeated once, together with

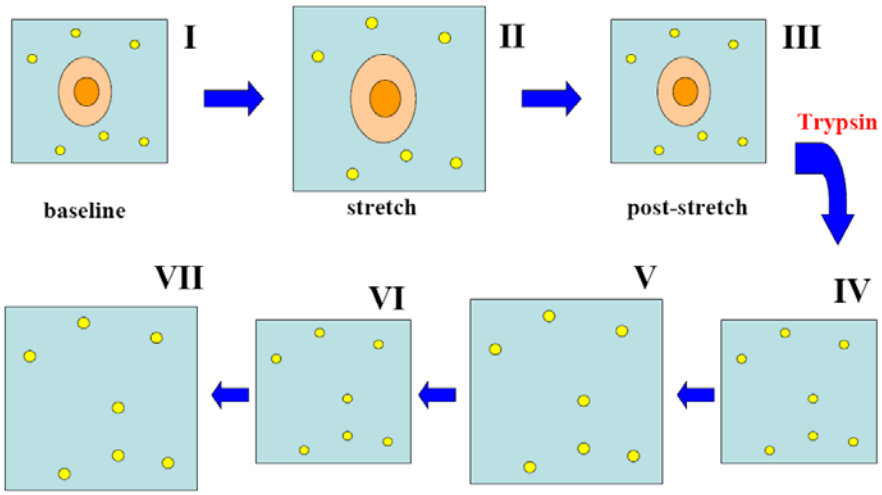

Fig. 5.2 Scheme of the traction microscopy protocol. A well containing a cell-cultured collagen gel was placed on the stretching device. I: Bright field and fluorescence images of an isolated cell were acquired. II: The well was stretched and bright field and fluorescence image acquisition was performed again. III: The stretch was released and two final bright field and fluorescence images of the cell were acquired. IV: After cell removal, a fluorescent image was recorded to assess the cell-free unstrained gel. V: The gel was stretched again, and a fluorescence image was recorded to observe the cell-free strained gel. VI-VII: Stretching-unstretching was repeated, together with fluorescence imaging, to measure stretch repetitivity and reversibility.

fluorescence imaging, to assess stretch repetitivity and reversibility (VI-VII). Additional fluorescence images of the stretched gel at intermediate strain levels were acquired to allow for posterior computation of large bead displacements. Whole sample displacements occurred when stretch conditions were changed. Therefore, due to required focus relocations, approximately 2 min elapsed between two successive fluorescence images. Cells that showed clear partial detachment from the gel substrate due to stretch were rejected.

Measurement of the stretch-induced contractile response

A first set of traction microscopy measurements was aimed at determining the contractile response of alveolar epithelial cells to substrate deformations of different amplitudes. Both force generation under stretch conditions and after stretch release was studied following the traction microscopy protocol described in Fig. 5.2. Wells containing cell-cultured collagen gels were subjected to mid (5.5%), high (11%) or no (0%) strains. Measurements were carried out in n=6 wells from different cell-gel samples for each strain level.

Actin staining

The role of actin polymerization on the stretch-induced contractile response was assessed by staining of F- and G-actin in an independent series of cells cultured on flexible-bottomed wells. The protocol for staining F- and G-actin is extensively described in Appendix C. For control wells, no stretch was applied before the staining protocol. For stretched cells, staining was carried out 2 min after starting stretch application (11% strain). For stretch-release cells, wells were previously stretched (11% strain) for 2 min, and staining started 2 min after stretch release. Images were taken in n = 6 wells for each condition.

Partial inhibition of MLC activity

In a second set of traction microscopy experiments we studied the role of the acto-myosin machinery in cell contractile response to stretch. MLC activity was partially inhibited pre-treating the cell culture with ML-7 (10 μM) for 30 minutes. Wells containing cell-cultured collagen gels were subjected to mid strain (5.5%) following the traction microscopy protocol previously described (see traction microscopy protocol). Measurements were carried out in n=6 wells.

Traction force recovery after stretch release

In a third set of traction microscopy experiments we assessed the time-course of traction force recovery after stretch release. Wells containing cell-cultured collagen gels were subjected to mid strain (5.5%) following the traction microscopy protocol previously described (see traction microscopy protocol). 2 min after stretch release, fluorescent images of the microbeads embedded near the surface of the gel were acquired at 1 image/min for 8 min. After this ime-course recording, the usual traction microscopy protocol was resumed. Measurements were performed in n=6 wells.

5.2.7 Traction microscopy data processing

Cell contour determination

Cell boundary was determined using a Sobel edge detector algorithm (Castleman KR, 1996) implemented in LabView (National Instruments, Austin, TX). The projected area of the cell (A) was computed as the area enclosed by the cell boundary.

Stretch computation

To compute applied gel strain $(\overline{S})$, the displacement field of the microbeads due to gel stretching was determined using the fluorescent images acquired after cell detachment (images IV and V,Fig. 5.2). The displacement field between fluorescence images was computed using the Image Correlation Method (Tolic-Norrelykke et al., 2002). Images were iteratively divided into smaller windows and the displacement field between a pair of images was obtained by identifying the coordinates of the peak of the cross-correlation function between each pair of windows. To allow for large displacement determination, fluorescence images of the gel stretched at intermediate strain levels were used. Pairs of images of successively increasing strain were compared, and the final displacement field was computed as the cumulative displacement from all intermediate fields. Two stretch fields, S_x (x,y) and S_y (x,y) (Fig. 5.3B and C), were computed from the displacement field (Fig. 5.3 A), corresponding to the point-by-point stretch in the x and y directions. The following equations were used

$$S_y(x,y) = \frac{D_y(x, y+\Delta y) - D_y(x,y)}{\Delta y} \qquad S_x(x,y) = \frac{D_x(x+\Delta x, y) - D_x(x,y)}{\Delta x}$$

where D_x (x,y) and D_y (x,y) correspond to each of the two components of the displacement field at (x,y) coordinates. These equations equal the gradient of the displacement field in the x and y directions, respectively. To perform the computation, a (5×5) north or west gradient filter was used. The spatial resolution of the obtained stretch fields was 2.6 µm. To obtain a single representative value from each stretch field, data points of S_x(x,y) or S_y(x,y) were pooled into a stretch probability distribution (Fig. 5.3 E and F). Average $\overline{S_x}$ and $\overline{S_y}$ were computed as the median values of these distributions. $\overline{S}$ was computed as the mean between $\overline{S_x}$ and $\overline{S_y}$. For calibration of the stretching device, computation was performed using the whole stretch field. For determination of $\overline{S}$ in cell stretching experiments, the median value was computed using only points laying into the region of the stretch field which corresponded to the location where the cell had been adhered. To define this region, the previously determined cell contour was enlarged by 12 µm, which thus provided enough data for stretch statistics.

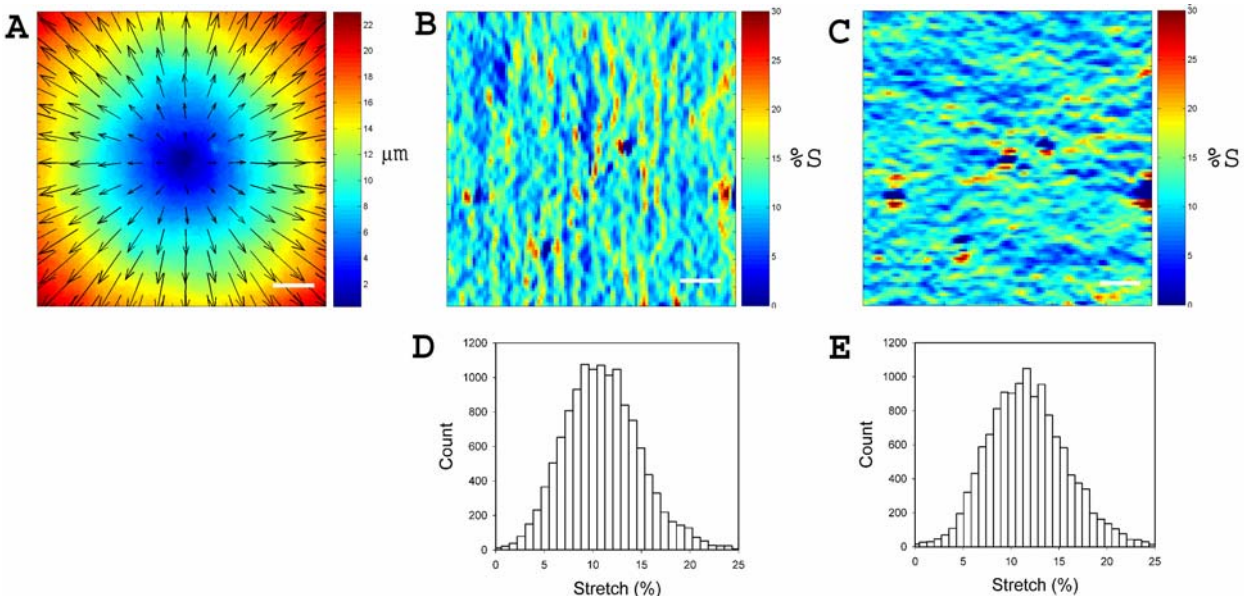

Fig. 5.3- *A:* Displacement field of a collagen gel subjected to 11% stretch. *B* and *C*: Corresponding strain fields S_x(x,y) and S_y(x,y) computed from the displacement field in shown in *A*. *D* and *E:* Histograms of the stretch distribution. Plots are pooled stretch data of the corresponding stretch fields S_x(x,y) and S_y(x,y) shown in *B* and *C*. Color scales indicate the magnitude of displacements and stretch. Arrows in the figure depict the direction and relative magnitude of displacement. Displacements and strains were calculated with 2.6 µm spatial resolution. Scale bar is 20 µm.

Validity parameters

To measure the goodness of each cell stretching experiment, two validity parameters were defined and an acceptance threshold value was established for each of them. To assess stretch biaxiality, the coefficient of variation (CoV = SD/mean) between $\overline{S_x}$ and $\overline{S_y}$ was computed. Stretch repetitivity in each measurement was assessed by measuring CoV between $\overline{S}$ from two successive stretch applications (images V and VII, Fig. 5.2). For each single experiment, the values of the validity parameters were computed and a given experiment was accepted only if both values fell within the validity range: 25% and 5% for stretch biaxiality and stretch repetitivity, respectively.

Traction field computation

To compute traction forces (*T*) exerted by the cell on the substrate, the displacement field of the gel substrate was first determined from the stored fluorescent bead images. The displacement field between each fluorescence image and the cell-free image corresponding to the same strain level was computed using the Image Correlation Method (Tolic-Norrelykke et al., 2002). The traction field (*T*(x,y)) was computed from the gel Young's modulus of the gel at the corresponding strain level and the displacement field, using Constrained Fourier Transform Traction Cytometry (CFTTC) (Butler et al., 2002). In traction field computations, the cell boundary estimated with the edge detector algorithm was enlarged by 3 μm (see section X.X for discussion). Cells with unclear boundary or displacement fields incongruent with cell shape were rejected. The spatial resolution of the displacement and traction maps was 2.6 μm.

Total force and net contractile moment computation

For each traction field, the total force magnitude (*F*) was computed by integrating the magnitude of *T*(x,y) over the projected area of the cell (Gaudet et al., 2003). The net contractile moment (*M*) was computed as defined by Butler and coworkers (Butler et al., 2002). *M* is a measure of the cell contractile strength that can be used as an index of cytoskeleton tensile stress (prestress) (Wang et al., 2002).

5.2.8 Statistics

Unless stated otherwise, data are reported as mean ± SE. One-way analysis of variance was used to study changes in E due to gel stretch. Two-way repeated measures analysis of variance was used to test whether stretch modified cell contractile force generation, cell area or net contractile moment. Comparison between means of baseline F for ML-7 pre-treated and non-pretreated cells was carried out with unpaired t test. On force recovery experiments, comparison between means of F at the initial and final time points was carried out with paired t test. Statistical significance was assumed at $P < 0.05$.

5.3 Results

5.3.1 Calibration and performance of the stretching device

An example of the displacement and strain fields of a stretched collagen gel is shown in Fig. 5.3. Displacement vectors exhibited radial direction pointing away from the centre of the field and their magnitude increased radially (Fig. 5.3 A). Stretch was approximately constant all over the field, although it displayed random deviations (Fig. 5.3 B and C) with local stretch values following a wide log-normal distribution (Fig. 5.3 D and E). When the stretch was released no plastic deformations were observed in the gel, and the noise traction found comparing two unstrained or strained images of the gel was low (Fig. 5.4).

The calibration of the stretching device is displayed in Fig. 5.5. A linear relationship between pressure and strain was found, with a maximum deformation of 13.5% for a vacuum pressure of 350 mmHg. The error bars indicate the variability among gels (n=5). As shown in Fig. 5.5 right, the system was highly equibiaxial with discrepancies < 10% between S_x and S_y.

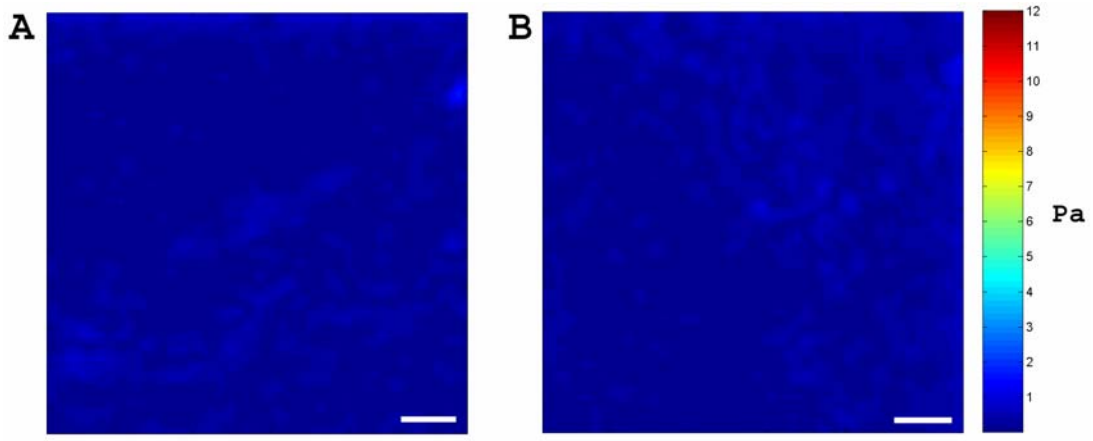

Fig. 5.4 - Noise traction fields computed from two fluorescence images of the unstrained (A) and the strained (B) collagen gel before and after a stretch application. Color scale indicates the magnitude of traction, using the same scale as in Fig. 5.7. Arrows depict the direction and relative magnitude of traction. Tractions were calculated with 2.6 μm spatial resolution. Scale bar is 20 μm

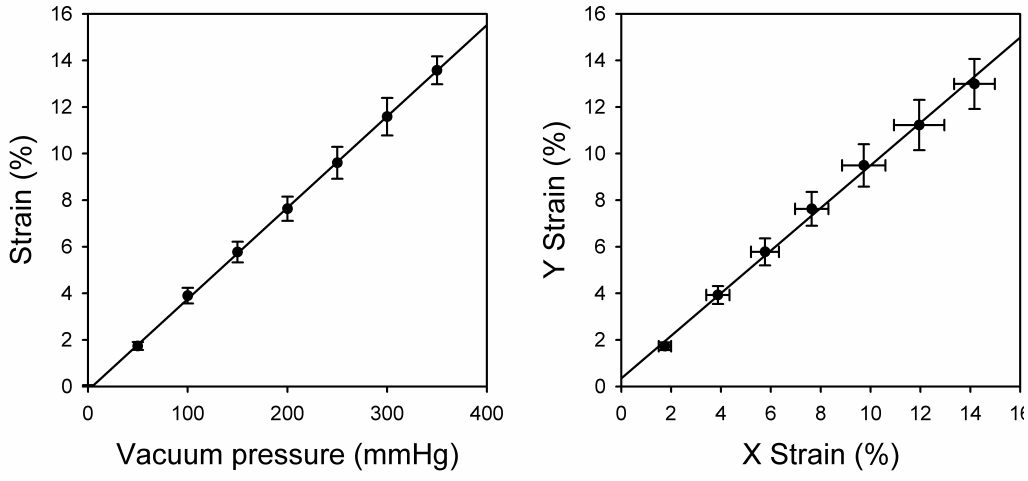

Fig. 5.5 - Calibration of the stretching device. Stretch was computed from fluorescence images of the top of stretched collagen gels (n=5). The pressure-strain curve was linear (left) and biaxial (right) up to 13.5% deformation. Data are mean ± SE.

Young's modulus of collagen gels displayed a strong and significant dependence on applied strain ($P < 0.05$), as shown in Fig. 5.6. E of unstrained gels was 22.7 ± 5.5 Pa (mean ± SD), whereas application of 5.5% and 11% strain increased the measured E by 2-fold and 5.5-fold, respectively. CoV of E within gel samples was maximal for high strain, and displayed an average value of 75%. Maximal variability between gel samples (CoV= 46%), which was also maximal for high strain, was lower than intra-sample variability. E was found to be similar on successive stretch applications of the same strain level. Average E obtained on the first high strain application was 102 ± 45 Pa, whereas average E on the last high stretch application was 108 ± 79 Pa (P=0.9). The same behavior was observed on unstrained gels, yielding E values of 24 ± 3.5 Pa on the first E measurement and 19 ± 1 Pa after five stretching-unstretching cycles (P=0.25).

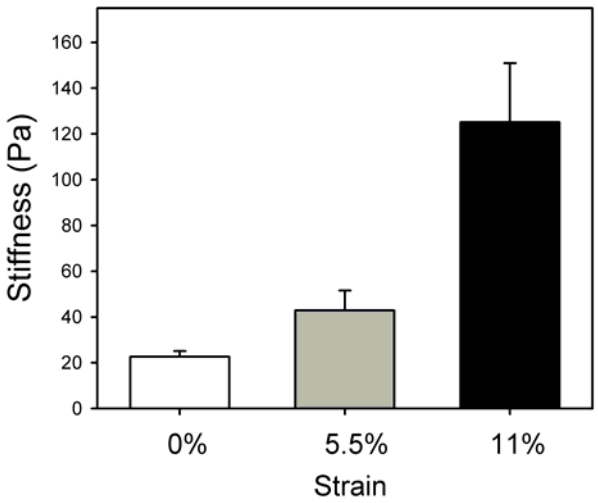

Fig. 5.6 - Strain-hardening of collagen gels. Young's modulus of collagen gels (n=5) subjected to 0% (white bar), 5.5% (gray bar) and 11% (black bar) strain. Data are mean ± SE.

Applied strain, together with values of the validity parameters could be computed for each single measurement performed on cells. For experiments carried out with mid strain levels, average strain yielded 5.5 ± 0.3 % (mean ± SD). The average strain was 10.3 ± 2.1 % (mean ± SD) in experiments where high strains were applied. Average CoV between S_x and S_y, which provided a measurement of stretch biaxiality, was 14 ± 9 % (mean ± SD). Stretch repetitivity, computed as CoV of two successive stretch applications, was 1.4 ± 0.9% (mean ± SD).

5.3.2 Mapping of traction forces

Traction fields of an A549 cell before, during and after being subjected to 5.5% strain are shown in Fig. 5.7. Under baseline conditions the cell exhibited a modest contractile tone with weak traction forces mainly located along the cell periphery and pointed towards the nucleus (Fig. 5.7, left). Little traction was observed beneath the central region of the cell. Stretch application induced a marked increase in traction forces, although force distribution and direction remained similar (Fig. 5.7, mid). Stretch release resulted in traction force magnitude lower than baseline without marked changes in force direction or distribution (Fig. 5.7, right).

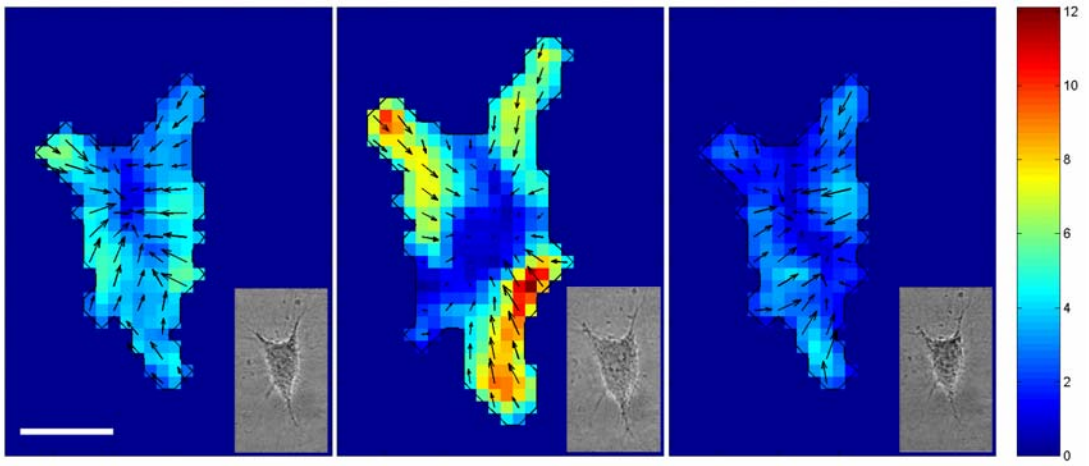

Fig. 5.7 Mapping of alveolar epithelial cell contraction induced by stretch. Traction field of an A549 cell before (left), during (mid) and after (right) stretch application. Insets are bright field images of the cell in the corresponding stretch configurations. Cell boundary drawn from the bright field image is shown as a black line. Color scales indicate the magnitude of traction force (Pa). Arrows depict the direction and relative magnitude of traction force. Tractions were calculated with 2.6 μm spatial resolution. For clarity, arrows in the figure are displayed with 7.8 μm spacing. Scale bar is 20 μm.

5.3.3 Effect of stretch on cell contractile forces

Total force magnitude of A549 cells under baseline conditions was 5.5 ± 0.8 nN. The area of cells was 813 ± 42 μm^2 corresponding to an average traction of 6.77 ± 1.1 Pa. Stretch induced significant increase in F ($P<0.01$) (Fig. 5.8) and M ($P<0.01$) (Fig. 5.9). 5.5% strain resulted in 45% increase ($P=0.25$ vs baseline) in F and 87% increase ($P=0.15$ vs

baseline) in *M*, whereas 11% strain induced a significant 2-fold increase (P<0.05 vs baseline) in *F* and 2.4-fold increase (P<0.01 vs baseline) in *M*. The area of cells exhibited a significant increase (P<0.001) due to substrate deformation (Fig. 5.10). *A* increased by 12% (P<0.001 vs baseline) and 24% (P<0.001 vs baseline) for mid and high strains, respectively. When the substrate was relaxed to its initial conformation, *F* and *M* were found to be lower than in baseline conditions (P<0.001). After stretch release, *F* decreased to 61% (P<0.05) and 33% (P<0.001) of its baseline value for mid and high strains, respectively, and *M* decreased to 59% (P=0.15) and 34% (P<0.01). For both strain levels, *A* was reduced by ~6% (P<0.01) when the substrate returned to its unstrained conformation. Little variations were observed on *F*, *M* or *A* throughout the whole experiment when no stretch was applied to the cells (P=0.39 for *F*, P=0.11 for *A*) (Fig. 5.8, Fig. 5.9, Fig. 5.10).

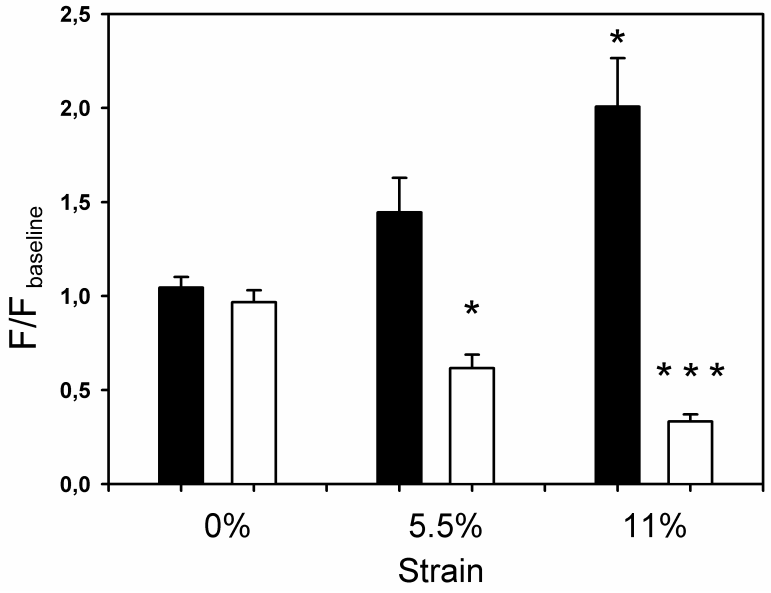

Fig. 5.8 - Contractile response induced by stretch on A549 cells. *F* values are presented as relative changes versus baseline *F*. Cells were subjected to 0% (n=6, left bars), 5.5% strain (n=6, mid bars) or 11% strain (n=6, right bars). Black bars correspond to stretch configuration and white bars to post-stretch configuration. * and *** indicate p<0.05 and p<0.001 vs baseline conditions, respectively.

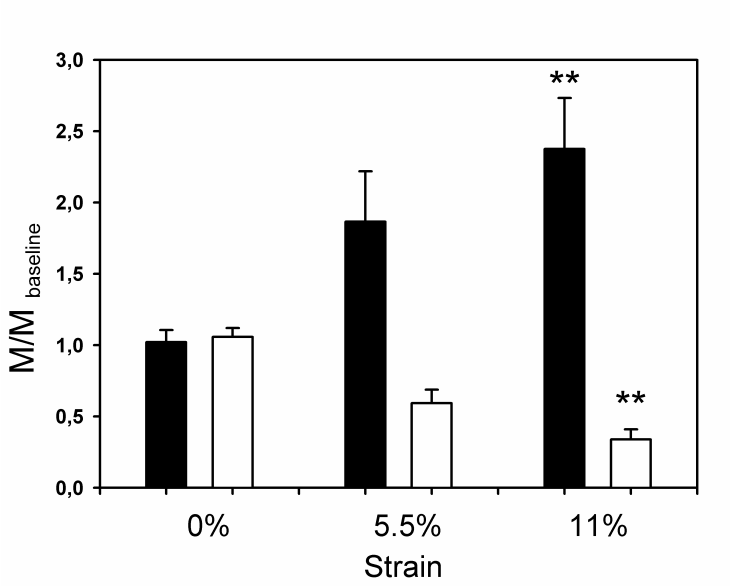

Fig. 5.9 - Contractile response induced by stretch on A549 cells. *M* values are presented as relative changes versus baseline *M*. Cells were subjected to no 0% (n=6, left bars), 5.5% strain (n=6, mid bars) or 11% strain (n=6, right bars). Black bars correspond to stretch configuration and white bars to post-stretch configuration. ** indicates $p<0.01$ vs baseline.

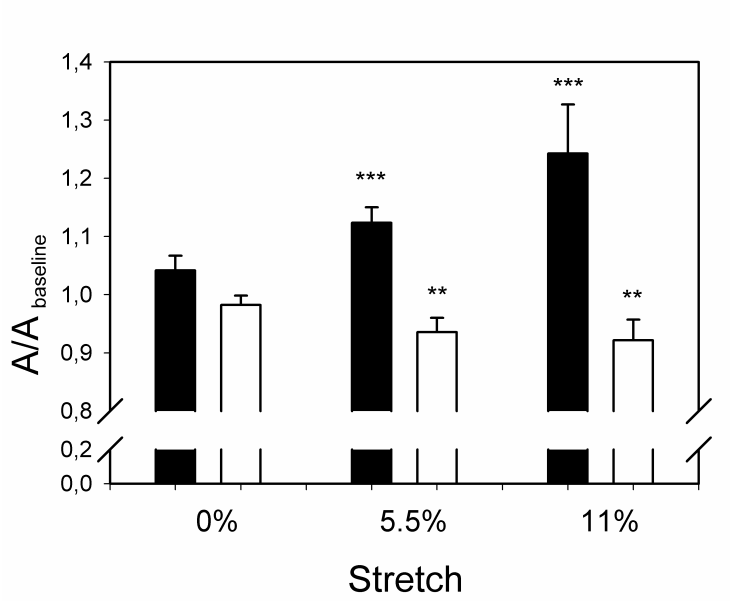

Fig. 5.10 - Changes in cell area induced by substrate stretching on A549 cells. *A* values are presented as relative changes versus baseline *A*. Cells were subjected to no strain (n=6, left bars), 5.5% strain (n=6, mid bars) or 11% strain (n=6, right bars). Black bars correspond to stretch configuration and white bars to post-stretch configuration. ** and *** indicate $p<0.01$ and $p<0.001$ vs baseline.

5.3.4 Contribution of the actin cytoskeleton and the acto-myosin machinery

F/G-actin fluorescence ratio was 3.8 ± 0.4 in baseline conditions (Fig. 5.11). No significant differences were observed in 11% stretched cells (7% decrease, P=0.42) and stretch-release cells (6% decrease, P=0.31).

Inhibition of MLCK with ML-7 decreased baseline traction force of alveolar epithelial cells by 55 % ($P < 0.05$). Pre-treated cells exhibited a response to stretch significantly different from that observed in non-pretreated cells ($P < 0.05$) (Fig. 5.12). 5.5% strain induced a 2.4-fold increase in F ($P < 0.01$ vs increase in non-pretreated cells). In addition, F was nearly recovered after stretch release (92% of baseline) in pretreated cells.

Time-course of F after stretch release exhibited a slow but marked force recovery, reaching values of F similar to baseline 8 min after stretch release (Fig. 5.13).

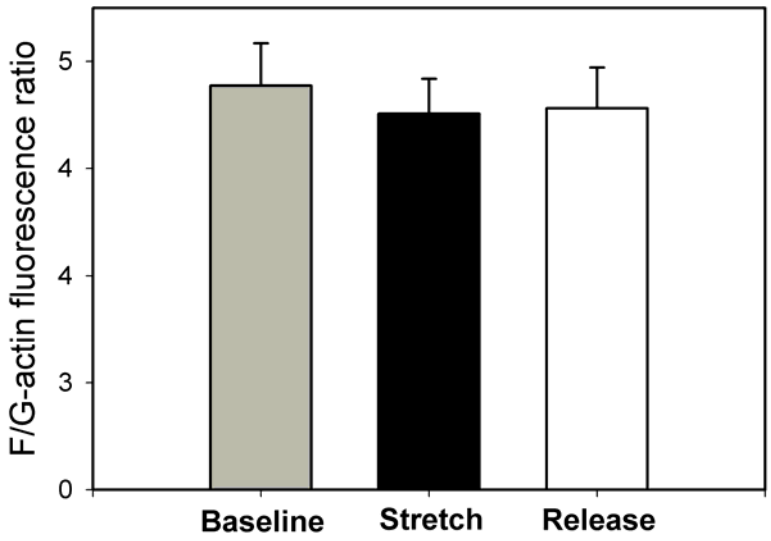

Fig. 5.11 - Changes in F/G-actin ratio induced by stretch on A549 cells. Staining protocol was carried out before stretch (gray bar, n=5), during 11% strain (black bar, n=5) or after strain release (white bar, n=5).

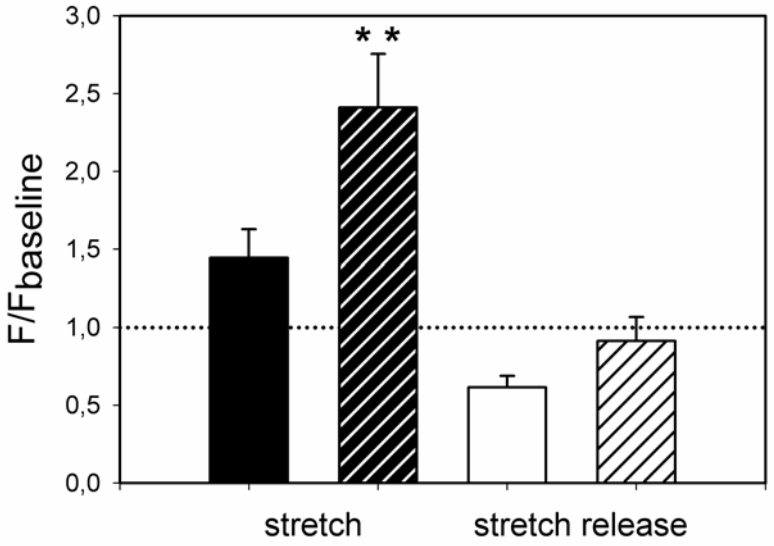

Fig. 5.12 - Effect of inhibition of MLCK on the contractile response induced by stretch. *F* values are presented as relative changes versus baseline *F*. Cells were subjected to 5.5% strain (black bars) and the stretch was subsequently released (white bars). Solid bars correspond to non-pretreated cells (n=6) and crossed bars to ML-7 pre-treated cells (n=6). Dotted line corresponds to baseline *F*. ** indicates $p<0.01$ vs stretch-induced relative increase in control conditions (solid black bar).

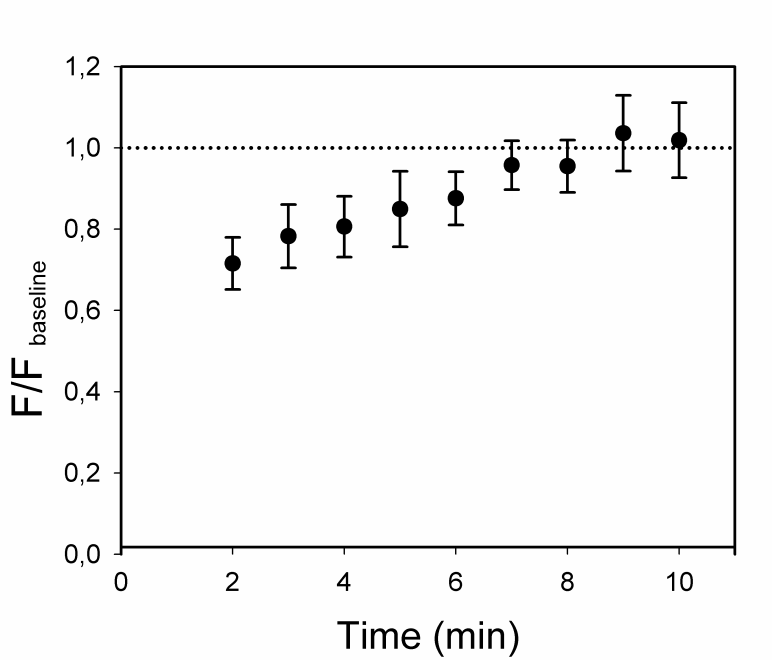

Fig. 5.13 - Time-course of *F* recovery after stretch release. *F* values are presented as relative changes versus baseline *F*. Cells (n=6) were subjected to 5.5% strain and the stretch was subsequently released. Initial time corresponds to instant of stretch release. Dotted line corresponds to baseline *F*.

5.4 Discussion

In this study we measured traction forces of alveolar epithelial cells subjected to equibiaxial stretch with a novel experimental approach. Stretch application induced significant and amplitude-dependent increase in traction forces exerted by A549 alveolar epithelial cells. Stretch release resulted in significant decrease of traction forces with respect to baseline conditions. The distribution of traction forces before, during and after stretch application was mainly located along the cell periphery and pointed towards the cell center. Stretch did not cause significant changes in actin polymerization. Reduction of MLC phosphorylation by inhibition of MLCK enhanced stretch-induced increase in traction forces and attenuated the decrease in traction force after stretch release as compared with nonpretreated cells. A549 cells exhibited slow recovery of contractility, reaching baseline levels 8 min after stretch release.

5.4.1 Substrate deformation pattern

The implemented experimental setup combines two previously established techniques: equibiaxial substrate stretching and traction microscopy. The substrate-stretching device was adapted from a previously described method, based on applying vacuum underneath a flexible-bottomed well (Trepat et al., 2004). The device also included a frictionless circular loading post placed under the flexible membranes, thus enabling preservation of the focal plane position, together with equibiaxial stretching (Brown, 2000). We applied equibiaxial stretches to alveolar epithelial cells because this pattern of cell deformation has been extensively used to obtain relationships between cell deformation and induced response in this cell type (Tschumperlin et al., 2000;Trepat et al., 2004;Cavanaugh, Jr. et al., 2001;Cavanaugh et al., 2006). Nevertheless, it must be kept in mind that alveolar epithelial cells are believed to experience heterogeneous deformations in vivo (Tschumperlin et al., 2000). The substrate-stretching device was designed to allow selection of applied stretch by changing the vacuum pressure underneath the flexible membrane. The selected stretch levels for our study corresponded to 11.3% and 23.2% increase in substrate area (ΔSA). Some studies report that actual cell strain is considerably lower than the strain experienced by the substrate (Liu et al., 1999). By contrast, other studies assume that substrate strain is completely transmitted to cells (Tschumperlin and Margulies, 1998). Using the relationship between ΔSA of basement membrane and lung

inflation volumes proposed by Tschumperlin and coworkers (Tschumperlin et al., 2000), we conclude that the stretches we applied corresponded to those undergone by alveolar epithelial cells in vivo at volumes corresponding to ~65% and ~85% of total lung capacity. It should be noted that electronic micrographs showed that type II alveolar epithelial cells remained relatively spared after high volume ventilation. This may indicate that type II cells experience smaller deformations that type I cells on account of their location in alveolar corners (Vlahakis and Hubmayr, 2005).

5.4.2 Collagen gel substrates

Alveolar epithelial cells were cultured at the top of type I collagen gels. The composition of this gel substrate resembles the extracellular matrix (ECM) to which alveolar cells attach in vivo, which is mainly composed of collagen IV. Nevertheless, the stiffness of our collagen gels is lower than that reported for some ECM, although both lay in the range soft substrates (Paszek et al., 2005). Interestingly, it has been reported that ECM properties may regulate cellular shape and adhesion (Yeung et al., 2005;Reinhart-King et al., 2005;Paszek et al., 2005). By contrast, we could not find large differences in cell shape or area between A549 cells on this study and on the previous study carried out on polyacrilamide gels with stiffness closer to that of ECM (Chapter 4)(Gavara et al., 2006). In addition, A549 cultured on collagen gels did exert traction forces onto their substrate and respond to mechanical and biochemical stimulus. On the other hand, collagen gels have been previously shown to display strain-hardening (Storm et al., 2005). Therefore, it is reasonable to think that ECM of alveolar epithelial cells will also stiffen under stretch. Accordingly, the collagen I substrate used in our experiments, which also exhibits strain-stiffening (Fig. 5.6), reproduces the mechanical conditions experienced *in vivo* by alveolar epithelial cells. Taking into account their composition, stiffness and strain-hardening behavior, collagen gels constitute a suitable gel substrate to study traction forces exerted by alveolar epithelial cells.

5.4.3 Traction microscopy to probe stretch-induced traction force generation

Collagen gels with embedded fluorescent microbeads were used as transparent and

elastic substrates for traction microscopy experiments. Contrary to polyacrylamide (PAA) gels commonly used for traction microscopy experiments, collagen gels attached firmly to the silastic membranes from the flexible-bottomed wells. This firm attachment made possible that the deformation undergone by the flexible membrane was fully transmitted to the collagen gel. Besides the different hydrogel used as cell substrate, our technical approach has other substantial differences from the method previously described by Munevar and coworkers to apply stretch and measure traction forces of adherent cells (Munevar et al., 2004). Munevar's method applied local not-biaxial strains to PAA gels by means of a blunted tip. Moreover, uncontrolled gel deformation and cell defocusing during stretch application did not allow for measurements of traction forces during stretch. Therefore, their method could only measure traction forces before and after local stretch application, and could not provide an estimate of the applied stretch. By contrast, our vacuum-driven setup enables application of the same level of biaxial stretch to the whole cell in a fully controlled way. In addition, the top surface of the collagen gel can be imaged both in unstretched and stretched configurations. This allows measuring the deformation of the gel induced by the attached cell both in baseline and stretch configurations. In addition, the collagen gel does not exhibit plastic deformations when it returns to its initial unstretched configuration (Fig. 5.4), thus enabling deformation of the gel induced by the adhered cell to be measured also after stretch release. Finally, collagen gels do not exhibit any degradation due to the trypsin added at the end of traction microscopy experiments to detach the cell. This enables acquisition of cell-free reference images, both for unstretched and stretched configurations. Importantly, these reference images are subsequently compared with the images acquired before cell detachment, enabling computation of absolute values of traction forces. Therefore, our experimental setup allows measurement of exerted traction forces before, during and after stretch application. Unfortunately, our experimental approach has one disadvantage. When the stretch is applied or released, the gel sample undergoes translocation and defocusing. For this reason, the studied cell has to be relocated in the field of the microscope and refocused, which takes ~2 min. Consequently, changes in traction forces occurring during the first two minutes after modification of stretch configuration can not be resolved.

5.4.4 Applied stretch and its computation

In previously described methods to stretch cell cultures, the relationship between mechanical actuation and resulting substrate deformation was first calibrated on cell-free samples. Subsequently, the calibration relationship was applied to cellular experiments (Tschumperlin and Margulies, 1998;Pourati et al., 1998;Rosenblatt et al., 2004). The drawback of this approach was that applied stretch could not be assessed for each single experiment. By contrast, we used the fluorescent microbeads embedded in the collagen gel to measure the strain level applied to each sample. By doing so, the probe intended to measure traction forces can also be used to compute gel stretch. A similar approach has been described by Trepat and coworkers, who used ferrimagnetic beads attached to the cells to measure both cell mechanical properties and monolayer stretch (Trepat et al., 2004). Nevertheless, the small number of probes used per sample could provide only a global index of monolayer stretch. By contrast, the high density of fluorescent probes imaged in traction microscopy experiments enables us to compute deformation and stretch fields on the region surrounding the cell with micrometer resolution (Fig. 5.3 A to C).

The deformation field induced by gel stretching is computed from the displacement of the fluorescent beads with the image correlation method (Tolic-Norrelykke et al., 2002), which is an algorithm extensively used in traction microscopy computations. Nevertheless, the displacements of the beads due to stretch are much larger than those induced by adhered cells and are too large to allow for their direct computation using the standard algorithms. Consequently a small variation was introduced in the fluorescence image acquisition protocol after cell detachment. Instead of directly comparing the fluorescent images of the unstretched and the stretched gel configurations, images of the gels successively stretched at intermediate strain levels were acquired, and the relative displacement of fluorescent beads was computed. Finally, the displacement field induced by stretch was computed as the sum of all the relative displacement fields. This computational approach resulted in increased random noise in the stretch-induced displacement field, although signal-to-noise ratio remained very low (Fig. 5.3 A). The stretch field was obtained by filtering the displacement field with a gradient filter. Since the gradient filter is a high-pass filter, random noise in the displacement field was enhanced in the stretch field. As a consequence, the stretch field displayed random deviations and the histograms of stretch exhibited a wide distribution (Fig. 5.3 D and E). Taking into account

the distribution of stretch values, a single representative stretch index for each field was computed as the median of the stretch distribution. Moreover, the stretch undergone by the studied cell was more precisely characterized by pooling only the stretch values corresponding to the region of the gel where the cell was adhered. The global stretch for the studied cell corresponded to the median of these pooled data. Together with cell-stretch, the experimental design also provided other resulting values, such as cell area, displacement field induced by the adhered cell, corresponding traction field, total force magnitude (F) and net contractile moment (M) exerted by the cell. These parameters were computed using common traction microscopy algorithms (Gavara et al., 2006), taking into account changes in Young's modulus of the collagen gel due to stretch. As described above, there are substantial methodological differences between our setup and common traction microscopy. Nevertheless, it should be noted that our experimental approach was designed to permit the use of TM algorithms to compute not only the contractile response exhibited by alveolar epithelial cells but also the applied stretch.

The experimental approach used to compute applied stretch and traction forces exerted by the adhered cells relies on two premises, namely repetitivity of applied stretch and non-plastic deformations of the gel. Therefore, care was taken to warrant the validity of these two assumptions for each experiment. To this end, the stretching protocol was extended to include acquisition of a second image for both unstretched and stretched cell-free gel configurations (Fig. 5.2 VI and VII). Comparison between the two images corresponding to the same configuration allowed for assessment of stretch repetitivity (Fig. 5.4 right) and non-plasticity (Fig. 5.4 left). Accordingly, experiments which did not fulfill both premises were discarded. On the other hand, stretch biaxiality was also computed to warrant correct transmission of stretch from the flexible membrane to the collagen gel. Once again, experiments with low biaxiality levels were discarded. The experimental approach was designed to study the same cell throughout the course of a single experiment. Accordingly, bright field images of the cell were acquired for each stretch configuration (Fig. 5.7 insets). This enabled compution of the cell's area and assessment of their changes during stretch application (Fig. 5.10). Consequently, whole cell attachment throughout the experiment was guaranteed by discarding cells that displayed partial detachment from the substrate or incongruent changes in area when the gel was stretched. Therefore, together with applied stretch and traction force values, a set of parameters such as stretch repetitivity and non-plasticity, stretch biaxiality and whole cell attachment were computed

to warrant the goodness of each single experiment.

5.4.5 Comparison of traction data with previous results on the same cell type

Total force magnitude of A549 cells was 10 times lower than that reported on a previous work from our laboratory (Gavara et al., 2006). Interestingly, that study was carried out on polyacrilamide gels, which were a 17-fold stiffer than the present collagen gels. This correlation between exerted force and substrate stiffness has been previously reported in epithelial cells by Saez and coworkers (Saez et al., 2005). Concretely, those authors reported that traction forces exerted by epithelial cells were proportional to the stiffness of their substrate, meaning that resulting displacement of the substrate induced by the adhered cell remained constant. Therefore, differences in substrate stiffness could account for the differences in contractility shown by different studies in the same cell type.

5.4.6 Effect of stretch on traction forces exerted by alveolar epithelial cells

Our TM measurements demonstrate that stretch induces increase in traction force of alveolar epithelial cells, but stretch removal results in lost of cell contractility with respect to baseline levels. Moreover, this behavior was found to be dependent on stretch amplitude. The stretch-induced increase in traction forces and its dependence on stretch amplitude could be explained by an effect discussed above, namely the correlation between traction forces and substrate stiffness reported in epithelial cells (Saez et al., 2005). Taking into account that stretch stiffens collagen gels, alveolar epithelial cells would respond to substrate stiffening by increasing traction force generation. Importantly, Saez and coworkers suggested that reinforcement of focal adhesions on stiffer substrates was responsible for the correlation they found. Nevertheless, the observed stretch-induced increase in traction forces may be too fast to be accounted for by focal adhesion reinforcement. Moreover, the aforementioned correlation could not explain the behavior of cell contractility observed after stretch removal, when the stiffness of the substrate returns to its baseline levels but cell traction forces exhibit a significant decrease with respect to baseline values. On the other hand, the observed decrease in traction forces after

stretch release could be attributed to partial cell detachment from the substrate, which would induce underestimation of forces exerted by the cell. By contrast, distribution of traction forces remained similar during and after stretch release, suggesting that cell-matrix attachments were not compromised by stretch application. Moreover, cell area did not exhibit large reductions after stretch release. Therefore, the observed decrease in traction forces in stretch-release conditions could not be attributed to cell detachment from the substrate due to stretch.

5.4.7 Mechanisms involved in the stretch-induced increase in traction forces

The structure of the cytoskeleton is believed to be regulated and stabilized by a preexisting tensile stress (prestress) carried by the actin filaments and partially balanced by focal adhesions to the ECM (Ingber, 2003). Cell prestress (*P*) can be computed from the contractile forces that adherent cells exert on their substrate. Accordingly, Wang and coworkers described three different metrics of cell prestress, one of them being the net contractile moment (*M*) (Wang et al., 2002). These authors stated that if the geometry of the adherent cell did not change appreciably during a contractile event, *P* should be proportional to *M*. Although this statement does not hold in our stretch measurements, we can still relate increases in *P* to increases in *M*. Specifically, if we assume that substrate stretch results in corresponding increases in cell area (Fig. 5.10) and that cell volume does not markedly change due to stretch (Pourati et al., 1998), then it follows on dimensional grounds that increases in *P* due to stretch will be proportional to increases in *M*. Therefore, the observed increase in *M* (Fig. 5.9) that we report indicates that stretch application increases cell prestress. Moreover, taking into account that cell area was only slightly reduced after stretch release (Fig. 5.10), the decrease in *M* also indicates that *P* decreased once the cell is relaxed to its initial configuration. It has been reported that changes in cell prestress result in changes in cell stiffness, following a nearly direct proportion (Wang et al., 2002). Accordingly, the changes in *P* induced by stretch that we observe should also result in changes on cell stiffness. Interestingly, a previous study from our laboratory showed that alveolar epithelial cells stiffen when subjected to stretch (Trepat et al., 2004;Trepat et al., 2006). Moreover, the strain-stiffening observed also displayed stretch-amplitude dependence. Therefore, the stretch-induced cell stiffening previously reported and may result from the increase in cell prestress.

The tensional prestress that stabilizes the whole cell is generated actively by the contractile actomyosin apparatus. In addition, passive contributions to prestress come from cytoskeleton distension through adhesions to the ECM and other cells, osmotic forces acting on the cell membrane, and forces exerted by filament polymerization (Ingber, 2003). The response to stretch of these active and passive contributions has not been completely assessed.

The response of the actin cytoskeleton to stretch application has been extensively studied in both reconstituted actin gels and cell cultures (Trepat et al., 2004;Gardel M.L., 2006;Fernandez et al., 2006). Cross-linked actin gels have been shown to stiffen non-linearly when subjected to stretch (Gardel M.L., 2006). Moreover, strain-stiffening of alveolar epithelial cells has been shown to be inhibited by disruption of the actin cytoskeleton with Latrunculin A (Trepat et al., 2004). Therefore, actin cytoskeleton distention could be considered the main responsible for the stretch-induced increases in cell stiffness and contractility. Stretch-induced changes in actin polymerization could also contribute to the observed increase in traction force generation. Nevertheless, measurements od F/G-actin ratio do not suggest a significant role of actin polymerization on the observed stretch-induced behavior. Conversely, our data may suggest that stretch could provide enough mechanical energy to disrupt or unfold some cytoskeletal crosslinks, thus resulting in slight decreases in F/G-actin ratio. Therefore, distention of the actin cytoskeleton without changes in actin polymerization may be considered one of the mechanisms responsible for the stretch-induced increase in cell prestress.

It has been postulated that disruption of actin-myosin interactions induces softening in stretched airway smooth muscle tissues (Fredberg et al., 1997), but this effect has only been suggested at the single cell level (Trepat et al., 2006). According to this hypothesis, the global change in cell prestress due to stretch application will result from two different contributions (Fig. 5.14). One the one hand, stretch-induced passive cytoskeleton recoil will contribute to increases in prestress. On the other hand, decrease in active cell contraction due to breaking of attached actomyosin crossbridges will reduce cell prestress. The final result of this prestress balance would depend on the number of attached actomyosin crossbridges before stretch. Therefore, in a highly activated cell, the decrease in prestress due to detachment of actomyosin crossbridges would exceed the

increase in cell prestress due to cytoskeleton distention, leading to prestress decrease and cell softening. On the other hand, in a relaxed cell, the passive increase in cell prestress would not be wholly counterbalanced by detachment of actomyosin crossbridges, resulting in prestress increase (Fig. 5.14).

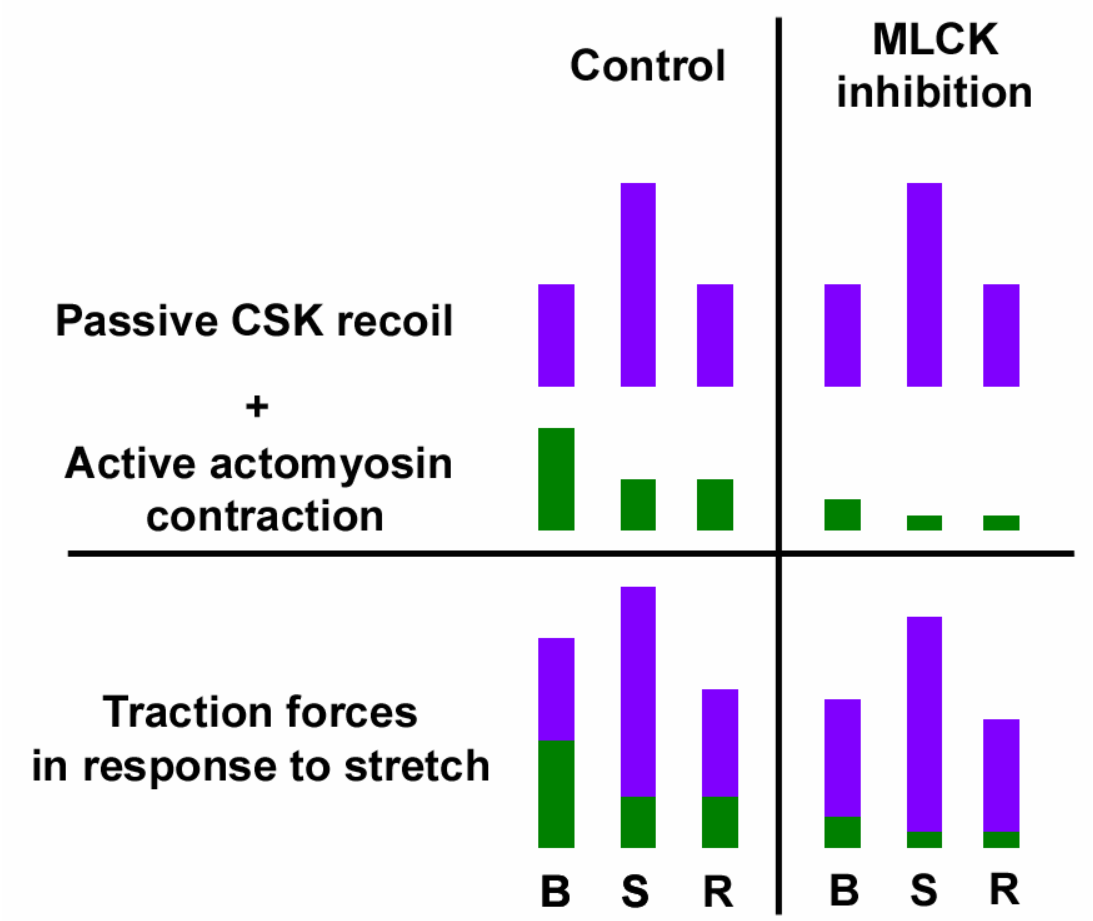

Fig. 5.14. Sketch to illustrate the suggested mechanisms contributing to cell prestress and their response to stretch. Blue bars represent the contribution of passive cytoskeleton recoil, whereas green bars represent active actomyosin contraction. B: Baseline, S: stretch, R: stretch release. The left bars correspond to control conditions and the right bars correspond to ML7 pre-treated cells, where the passive cytoskeleton contribution remains unchanged but the active actomyosin contribution has been reduced. In both conditions, stretch increases passive cytoskeleton recoil but reduces active actomyosin contraction. When stretch is released, cytoskeleton recoil returns to baseline levels whereas active contraction remains low. The different levels of baseline active contraction between control and ML7 conditions determine the different relative changes versus baseline observed when stretch is applied or released. As a result, ML-7 pre-treated cells display a bigger relative increase versus baseline than control cells.

Interestingly, our traction microscopy experiments fully support this hypothesis. Specifically, we relaxed our cells by inhibition of MLC kinase. When cells were subsequently stretched, relative force generation was significantly higher than in non-pretreated cells, suggesting that the decrease in prestress due to actomyosin detachment opposed less to the increase in prestress due to cytoskeleton distention (Fig. 5.14). Moreover, experiments on the same cell type showed that when cells were previously activated with a contractile agonist, stretch resulted in a decrease in cell stiffness (Trepat et al., 2006), thus further confirming the stated hypothesis. Changes in cell prestress after stretch release can also be predicted from our current hypothesis. On the one hand, the increase in the passive prestress component due to cytoskeleton distention would vanish once the stretch is released. On the other hand, broken actomyosin attachments may not be fully recovered (Fig. 5.13). As a consequence, the prestress balance would change again, displaying lower values than in initial conditions. Accordingly, our measurements on the net contractile moment show that prestress is lower than baseline early after stretch release. By contrast, stretch-release stiffness of alveolar epithelial cells was not significantly different from baseline values (Trepat et al., 2004;Trepat et al., 2006). Nevertheless, it should be noted that those measurements were carried out on cell monolayers adhered to stiff substrates. In addition, cells were reported to experience partial cell-cell or cell-matrix detachments, which has not be observed in our study. Therefore, breaking of tethering attachments could have taken place instead of or simultaneous to breaking of actomyosin crossbridges, resulting in different changes in prestress. In this connection, it has been suggested that observed mechanical properties of cells subjected to deformation may be influenced by alterations of cell–matrix adhesions (Wirtz and Dobbs, 2000). Similar to changes in prestress due to stretch, the relative amount of decreased prestress after stretch release may depend on the initial number of attached actomyosin crossbridges and the amount of broken crossbridges. Accordingly, cells relaxed by inhibition of MLC kinase displayed different behavior after stretch release, with force (F) values closer to initial levels.

5.4.8 Recovery of traction forces after stretch release

It has been previously shown that intracellular Ca^{2+} levels display a fast and transient increase after a single stretch application in alveolar epithelial cells (Wirtz and Dobbs, 1990). Increase in Ca^{2+} levels suggests phosphorylation of MLC kinase and subsequent activation of the actin-myosin contractile machinery, resulting in contractile

force generation. Accordingly, A549 cells displayed slow recovery of baseline force 8 minutes after stretch release, corresponding to 10 minutes after stretch application. This suggests that stretch-detached actomyosin crossbridges may be actively and progressively reattached by calcium-dependent signaling pathways. Therefore, alveolar epithelial cells may have a stretch-activated calcium-mediated signaling mechanism which enables active recovery of the contractility previously depleted by stretch. Stretch-activated calcium channels have been recognized for almost 15 years (Sachs, 1986). However, it remains unclear whether these stretch-sensitive channels are activated directly by conformational changes or indirectly via an intermediate mechano-sensitive protein which then opens the channel by a signaling pathway (Wirtz and Dobbs, 2000).

5.4.9 Cell contraction in cyclic stretch conditions and force balance in the cyclically-stretched lung

The aim of this work was to study the contractile response induced by a single step stretch on alveolar epithelial cells. Nevertheless, alveolar cells *in vivo* are constantly subjected to cyclic stretch, thus modifying the contribution to force generation of the passive and active prestress components aforementioned. In cyclic stretch conditions, the passive increase in traction forces induced by cytoskeleton distention will be experienced by alveolar cells only when the lung is inflated. On the other hand, our data suggest that cyclic stretch would mechanically decrease the amount of attached crossbridges while simultaneously triggering contraction-signaling pathways. The period of human breathing is ~4 sec, whereas observed stretch-induced calcium transients take place for 60 sec after stretch application (Wirtz and Dobbs, 1990). Moreover, contractile force recovery in alveolar epithelial cells is attained 10 minutes after stretch application. Therefore, the resulting activation level of the actin-myosin contractile machinery during cyclic stretch conditions can not be ascertained. Elucidation of the effect of cyclic stretch on alveolar epithelial cell contraction will require direct measurements of traction forces in long-time dynamic conditions.

The structural integrity of the alveolar epithelium is determined by a force balance between centripetal cytoskeletal tension and centrifugal cell-cell and cell-matrix tethering forces. Given that the epithelium undergoes cyclic stretch during breathing and mechanical ventilation, stretch-induced increase in centripetal forces is a central determinant of this

dynamic balance. Together, our results indicate that the force balance at the epithelial monolayer may be impaired during lung inflation, when cytoskeleton distention passively increases cell contractility. Moreover, stretch may induce active contraction by triggering contractile signaling pathways. Therefore, threatening of barrier integrity due to cell contraction also during lung relaxation may not be ruled out. Stretch has been shown to modify other components involved in the force balance of the alveolar epithelial monolayer, inducing cell stiffening (Trepat et al., 2004) and decreasing tethering adhesive forces (Cavanaugh, Jr. et al., 2001). Moreover, cyclic stretch at high strain levels induces increase in paracellular permeability (Cavanaugh et al., 2006). Therefore, our results and those reported by other authors support the hypothesis that stretching at high amplitudes may impair the force balance in the alveolar cell monolayer, thus compromising the mechanically ventilated lung.